UNIZIK JOURNAL OF AGRICULTURAL AND BIOSYSTEMS ENGINEERING

Journal homepage: https://journals.unizik.edu.ng/ujabe/

UJABE

April (2026), 1(2): 20-32

ISSN: 3141-2912

KINETIC EVALUATION OF THE EPOXIDATION OF LUFFA *CYLINDRICA* M. SEED OIL UTILIZING *LUFFA* FIBRE CATALYST

Prince Chinaemeze Iroabueke[a], *Kenechi Nwosu-Obieogu[a]

[a]*Chemical Engineering Department, Michael Okpara University of Agriculture, Umudike, Nigeria.*

**Corresponding Author's E-mail: kenenwosuobie@mouau.edu.ng*

Received: 15th January 2026; **Accepted:** 22nd January 2026; **Available Online:** 30th April 2026

ABSTRACT

The catalytic valorization of biomass offers a sustainable route for bio-epoxide production. Conventional epoxides produced with non-renewable catalysts pose environmental risks, exhibit poor biodegradability, and incur high production costs. However, *Luffa cylindrica* fibres have not been explored as precursors for heterogeneous epoxidation catalysts, and the epoxidation of *luffa* seed oil under catalytic kinetic regimes remains under-investigated. In this study, luffa fibre was sulfonated and converted into a heterogeneous nano-catalyst for the epoxidation of oleic-rich luffa seed oil (LSO). Catalyst activation increased the BET surface area from 294.28 to 353.29 $m^2 g^{-1}$ and expanded pore size from 2.69 to 3.13 nm, enhancing reactant diffusion and active site accessibility. Scanning Electron Microscopy (SEM) revealed nano-scale spherical agglomerates, while XRD confirmed crystallite formation (~45 nm) and improved lattice ordering. Fourier Transform Infra-Red (FT-IR) analysis verified the presence of acidic functional groups, and TGA demonstrated thermal stability up to ~420°C. Epoxidation achieved a maximum oxirane value of 5.21 mol at 65°C. Kinetic analysis showed pseudo-first-order behavior with rate constants of 0.0392–0.222 h^{-1} between 328–338 K, while thermodynamic parameters (Ea = 14.44 kJ mol^{-1}; ΔH = 14.44 kJ mol^{-1}; ΔS = −21.75 cal mol^{-1} K^{-1}) indicate an endothermic and ordered transition state.

Keywords: *luffa* oil, *luffa* fibre, kinetics, epoxidation

1.0 INTRODUCTION

Growing concerns over fossil resource depletion, environmental degradation, and carbon emissions have intensified interest in renewable feedstocks for chemical and polymer industries (Alvarez et al., 2025; Mukherjee et al., 2025). Biomass provides a compelling alternative owing to its abundance, carbon-neutrality, and alignment with green chemistry principles (Fernandes et al., 2025). Among biomass-derived feedstocks, plant seed oils are particularly attractive due to their biodegradability, low cost, and structural versatility (Varghese et al., 2025; Belaid et al., 2025). Their triglyceride matrices contain both saturated and unsaturated fatty acids, and the C=C bonds provide functional handles for chemical modification (Ho et al., 2022; Prasannakumar et al., 2024). Consequently, vegetable oils have been widely utilized as precursors for bio-based resins, polyols, coatings, adhesives, and composites, thereby supporting sustainable polymer production. *Luffa cylindrica*, a *cucurbitaceae* vine best known for its fibrous sponge, represents an emerging biomass with multifaceted value (Belaid et al., 2025; Jin et al., 2025). The mature fibres possess high porosity, mechanical strength, hydrophilicity, and a cellulose-rich framework, enabling applications in composites, filtration, adsorption, and biocatalytic supports. Surface functionalities further permit immobilization of enzymes and nanoparticles for heterogeneous transformations. Despite these advantages, luffa remains underutilized in chemical catalysis relative to other lignocellulosic residues (Fernandes et al., 2025). In parallel, luffa seeds yield an unsaturated oil that presents a promising precursor for bioepoxide and polymer synthesis, although

existing epoxidation studies are predominantly non-catalyzed (Lin et al., 2025; Khatoon et al., 2025; Ferraz-Caetano et al., 2025).

Epoxidation is the most widely adopted functionalization route for unsaturated vegetable oils and proceeds via reaction of peracids or active oxygen species across C=C bonds to form oxirane rings (Calabia et al., 2025; Rahman et al., 2025). Industrial processes commonly rely on in situ peracid formation from hydrogen peroxide and organic acids (Addli et al., 2025). Resulting epoxides serve as intermediates across chemical manufacture, yet conventional epoxidation suffers from corrosive media, excessive oxidant demand, long residence times, limited selectivity, and ring-opening byproducts (Nwosu-obieogu et al., 2022[a]; Kopal et al., 2022). Improving sustainability and efficiency requires kinetic understanding, as rates of peracid formation, mass transfer, and oxirane conversion dictate yield, selectivity, and oxidant utilization (Nwosu-obieogu et al., 2022[b]). Kinetic modelling further enables determination of rate constants, activation energies, and mechanistic pathways relevant to reactor design and scale-up (Nwosu-obieogu et al., 2024[a,b]).Catalyst choice is central to performance. Homogeneous catalysts, though efficient, exhibit corrosivity, waste generation, and poor recyclability (Baczewska et al., 2025). Biomass-derived heterogeneous catalysts offer advantages including tunable acidity, stability, and regeneration (Foroutan et al., 2022). Sulfonated carbonaceous catalysts in particular can promote both peracid formation and epoxidation (Nwosu-obieogu et al., 2022[a]). However, luffa fibres have not been investigated as precursors for heterogeneous epoxidation catalysts, nor has luffa oil epoxidation been evaluated under catalytic kinetic regimes. In theory, epoxidation generally occurs when the C=C double bonds in vegetable oil react with a peracid (often formed in situ from hydrogen peroxide and an organic acid such as acetic or formic acid) as shown in equation 1. This represents the conversion of unsaturated bond into an oxirane ring. This represents the conversion of unsaturated bond into an oxirane ring. This study addresses these gaps by developing a sulfonated heterogeneous catalyst from luffa cylindrica fibre for the epoxidation of luffa seed oil and establishing the reaction kinetics. The work integrates catalyst preparation, characterization, process evaluation, and kinetic modelling to enable dual biomass valorization and promote sustainable epoxide chemistry.

$$C = C + RCOOH \rightarrow Epoxide + RCOOH \quad \ldots\ldots\ldots\ldots\ldots\ldots\ldots\ldots\ldots 1$$

2.0 MATERIALS AND METHODS

2.1 Experimental site

The experiment was carried out in the Analysis Laboratory of **Chemical Engineering Department, Michael Okpara University of Agriculture, Umudike, Abia State, Nigeria**, where the preparation of the luffa fibre–derived catalyst, epoxidation of *Luffa cylindrica* oil, and subsequent physicochemical analyses were conducted.

2.2 Materials

Luffa seed oil, extracted from the optimal conditions reported in literature by Nwosu-obieogu et al., (2021), luffa fiber, acetic acid (85%), H_2O_2 (30wt%) Na_2CO_3, used for washing of the epoxidised oils.

2.3 Equipment

Magnetic heater, thermometer, feed funnel, measuring cylinder, separation funnel, three-necked bottom flask, stirring bulb, weighing balance, rotary evaporator, condenser

2.4 Epoxidation Procedure

Epoxidation was performed following Nwosu-Obieogu et al. (2024) with modifications. Luffa oil, acetic acid, and H_2O_2 (1:1.5:0.5 molar ratio) were charged into a three-neck reactor and refluxed at 65 °C under vigorous stirring. Hydrogen peroxide addition marked zero time. Identical reactant concentrations were used while varying reaction time, agitation, and catalyst loading. After each run, the product was washed with Na_2CO_3 solution and subjected to liquid–liquid extraction to recover the epoxide.

2.5 Analytical Techniques

2.5.1 Determination of Iodine Value and Oxirane Content

These analyses were performed on the epoxy product to assess the extent to which the original oil was converted into an epoxide.

2.5.2 Iodine Value Determination

Iodine value was determined by the Wijs method, dissolving the oil and titrating with sodium thiosulfate against a reagent blank. Iodine value of epoxidized samples was calculated after analysis using Eqn. 2:

$$IV = \frac{(B-S)\times M\times 12.69}{W} \quad \ldots\ldots\ldots\ldots\ldots\ldots\ldots\ldots\ldots\ldots.. 2$$

Where: IV - Iodine value, S - Vol. of $Na_2S_2O_3$, B - Vol. of $Na_2S_2O_3$ (blank)
W - Wt. of sample (g), M - Molarity of the $Na_2S_2O_3$

2.5.3 Oxiraine value determination

Oxirane oxygen was determined by titrating with hydrobromic acid in acetic acid, and OO was calculated from halogen reagent consumption. The Oxirane Oxygen Content of the analyzed samples was calculated using Eqn. 3:

$$OV = \frac{(B-S)\times M\times A_o\times 100}{1000W} \quad \ldots\ldots\ldots\ldots\ldots\ldots\ldots\ldots\ldots\ldots\ldots 3$$

Where: S - Vol. of NaOH used (ml), B - Vol. of NaOH used blank (ml), M - Molarity of NaOH, W - Wt. of sample (g), A_o - Atomic weight of O_2

2.6.1 Kinetics study of LSO epoxidation

The rate of the peracid formation was chosen as the rate-determining step; according to Nwosu-obieogu et al. (2024[a]), it can be expressed in equation 4 as:

$$\frac{d[EpOA]}{dt} = k([H_2O_2] - [EpOA])[RCOOH]_0 \quad \ldots\ldots\ldots\ldots\ldots\ldots\ldots\ldots\ldots\ldots\ldots \mathbf{4}$$

where EpOA is the epoxidized oil, the subscript 'o' is the initial concentration, $[H_2O_2]$ and $[RCOOH]_o$ is the initial H_2O_2 and acetic acid concentrations, and k is the epoxidation rate constant. Integrating eq. 4 gives equation 5. The reaction rate constant can be evaluated from the difference in OOC during the epoxidation reaction.

$$ln\{[H_2O_2]_0 - [EpOA] = -k_{EP}[RCOOH]_0\, t + ln\{[H_2O_2]_0 \quad \ldots\ldots 5$$

According to eq. 5, the plot of $ln\{[H_2O_2]0$-[EP] vs. time will give a straight line; the reaction rate constant (k) is determined from the slope.

2.7 Thermodynamic study of LSO

The enthalpy of activation ΔH is determined using equation 6:

$$\Delta H = E_a - RT \quad \ldots\ldots 6$$

where E_a is the activation energy, T is the absolute temperature, and R is the universal gas constant (8.314 J $mol^{-1}K^{-1}$). The activation entropy ΔS is determined using equation 7:

$$k = \frac{RT}{Nh} e^{\Delta s/R} e^{-E/RT} \quad \ldots\ldots 7$$

Where k is the Boltzmann constant (1.38 X $10^{23}JK^{-1}$), h is Planck's constant (6.63 X 10^{-34} Js), ΔS is the activation entropy, and N is the Avogadro's constant.

3.0 RESULTS AND DISCUSSION

3.1 Oil characterization

3.1.1 Physicochemical characterization of the *luffa* oil

Table 1 summarizes the physicochemical properties of raw luffa seed oil (LSO). The oil showed an acid value of 4.83 mg KOH/g, FFA of 2.41%, and a high iodine value (93.51 mg I_2/g), confirming suitability for epoxidation. Its viscosity and specific gravity indicate poor flow behavior, while low moisture favors stability. The peroxide and saponification values suggest oxidative stability and moderate molecular weight, consistent with previous luffa oil reports (Oyelaran et al., 2022; Nwosu-obieogu et al., 2025).

Table 1: Physicochemical properties of luffa oil

Physicochemical properties	***Luffa* oil**
Moisture content (%)	0.25
Kinematic viscosity @ 40°C (mm^2s-1)	52.05
Refractive index @ 31°C	1.4714
Acid value(mgKOH/kg)	4.83
Free fatty acid (mgKOH/kg)	2.415
Saponificationvalue (mgKOH/kg)	123
Peroxide value(meq/kg)	3.641
Specific gravity	0.956

Iodine value(mg I_2/g)	93.51
Molecular weight (g/mol)	1907.99
Ester value (%)	87.87

3.1.2 Fatty acid profile of the luffa oil

The fatty acid composition of luffa oil was analyzed using gas chromatography The analysis revealed that the oil contains approximately 13.55% saturated fatty acids and 70.87% unsaturated fatty acids. Oleic acid was identified as the dominant component, accounting for 61.5% of the total fatty acid profile, followed by linoleic acid at 9.82%. Based on this distribution, luffa oil can be classified as an oleic-rich feedstock, similar to other oils commonly utilized for biodiesel and biolubricant production (Oyelaran et al., 2022; Zhou et al., 2024). (Zhang et al., 2021).

3.1.3 FT-IR profile of the luffa oil

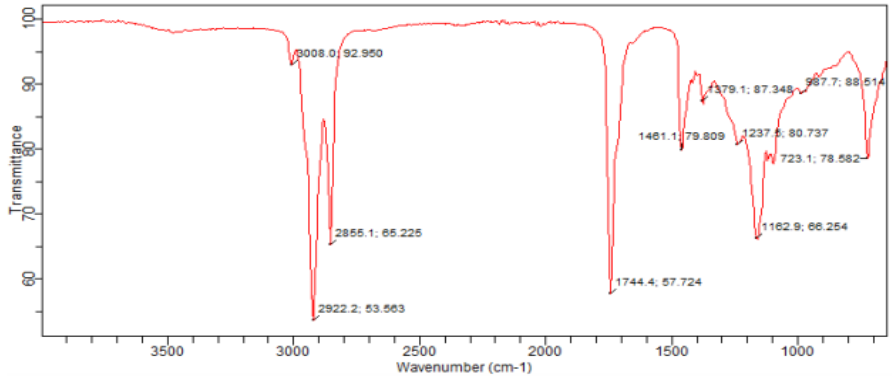

Fig. 1: FT-IR analysis of the *luffa cylindrica* oil

Figure 1 shows the FT-IR spectrum of luffa seed oil. Absorptions at 3008 cm^{-1} (O–H), 2922–2855 cm^{-1} (C–H), and 1744 cm^{-1} (C=O) confirm polyphenolic and ester functionalities, while the 1237 cm^{-1} band corresponds to C–O–C stretching. Peaks at 987 and 723 cm^{-1} indicate alkene groups, confirming triglyceride unsaturation. These observations align with reported luffa oil spectra and support its suitability for coatings and polymer applications (Zhou et al., 2024; Nwosu-obieogu et al., 2025).

3.2 Synthesized luffa catalyst characterization

3.2.1 FT-IR analysis

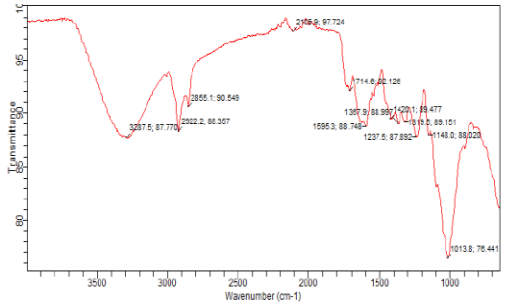

Fig 2a: luffa fiber (FT-IR)

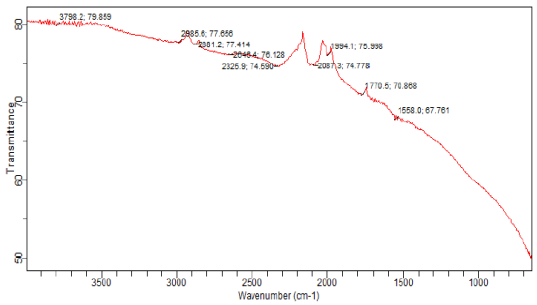

Fig 2b : FT-IR of the luffa fibre catalyst

3.2.2 SEM analysis

Figure 2a shows the FT-IR spectrum of untreated *Luffa cylindrica* fiber, exhibiting characteristic lignocellulosic bands from cellulose, hemicellulose, and lignin. A broad absorption at 3287 cm^{-1} corresponds to O–H groups involved in hydrogen bonding, while peaks at 2922 and 2106 cm^{-1} reflect aliphatic C–H stretching. The band at 1595 cm^{-1} suggests C≡C stretching, whereas absorptions at 1715–1238 cm^{-1} are assigned to carbonyl groups (esters, ketones, or acids). A sharp peak at 1014 cm^{-1} indicates C–O stretching of alcohols and esters, confirming polysaccharide and lignin functionality, consistent with reported spectra of plant fibers. Figure 2b presents the FT-IR profile of the luffa fiber-derived nanocatalyst. A strong O–H stretch at 3798 cm^{-1} indicates hydroxylated surfaces, while bands at 1994 and 1558 cm^{-1} correspond to carboxyl and C=C functionalities. The absorption at 1771 cm^{-1} suggests Al–OH–Si linkages, and the 2326 cm^{-1} band is attributed to carbonate species from CO_2 adsorption. These features agree with previous studies on green nanocatalysts used in luffa oil transesterification (De Souza et al., 2023; Paula et al., 2022).

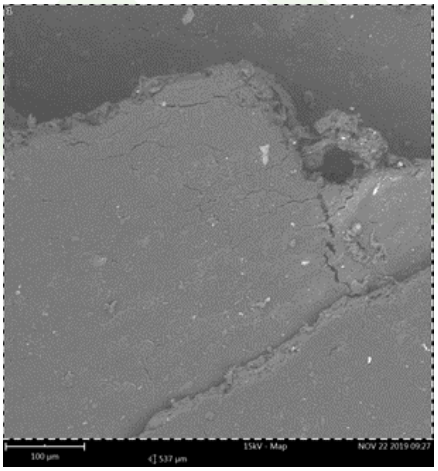

Fig. 3a SEM of the luffa fibre

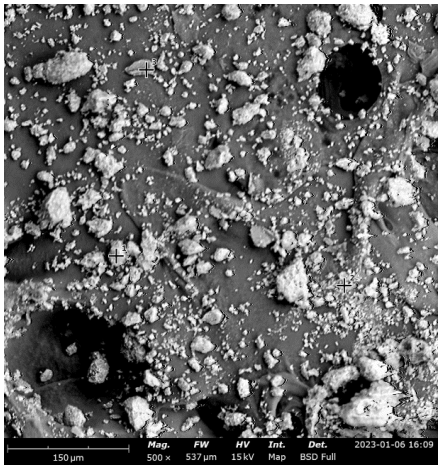

Fig. 3b. SEM of the catalyst

The SEM image of untreated *Luffa cylindrica* fiber (Fig. 3a) shows a compact, smooth surface consistent with an intact lignocellulosic framework. In contrast, Fig. 3b the synthesized

nanocatalyst displays fine, nearly spherical particles with visible agglomeration due to high surface energy and strong particle–particle interactions. Such clustering behavior and morphological features align with previous reports on treated and untreated luffa fibers for composites and on nanoscale catalysts synthesized from plant biomass (de Souza et al., 2023; Paula et al., 2022).

3.2.3 XRD analysis

XRD analysis (Figures 4a,b) shows structural changes from raw *Luffa cylindrica* fiber to the nanocatalyst. The untreated fiber exhibits a peak at 2θ ≈ 27° corresponding to silicon oxide and aluminum phosphate in kratochvite-type structures. Activation shifts the peak to 32.1°, indicating enhanced crystallinity and tetragonal phase stabilization. The mean crystallite size, estimated via the Debye–Scherrer equation, is ~45 nm, consistent with particle size data (40–100 nm), aligning with previous reports on luffa fiber-based composites and nanostructured materials (de Souza et al., 2023; Paula et al., 2022).

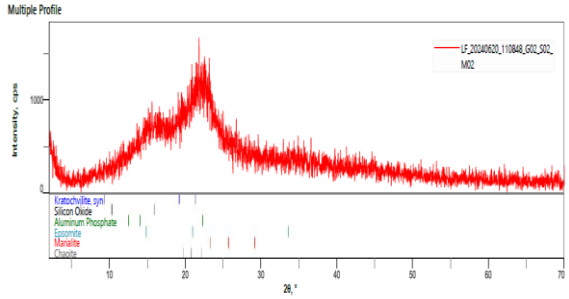

Fig. 4 a XRD of the luffa fibre

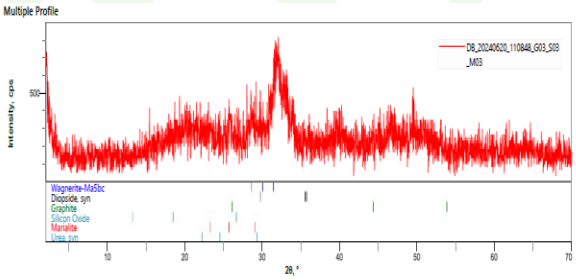

Fig. 4 b XRD of the nano catalyst

3.2.4 BET analysis

Table 3 shows that luffa-derived catalyst activation and nano-conversion significantly increased surface area, pore diameter, and volume, enhancing reactant diffusion and access to active sites. These structural improvements promote more efficient triglyceride–catalyst interactions, supporting transesterification, consistent with previous studies on luffa fiber applications in biosorption and biomass valorization (Santos et al., 2024; Countinho et al., 2024).

Table 3: Catalyst's physical properties

Parameters	Luffa fibre	Luffa nanocatalyst
Pore size (nm)	2.690	3.130
Surface area (m^2/g)	294.276	353.287
Total pore vol. (cm^3/g)	25.12	25.13

3.2.5 TGA analysis

TGA assessed the thermal behavior of Luffa cylindrica-derived nanocatalyst (Figures 5a, b). Initial weight loss between 300–400 °C corresponds to cellulose decomposition. The endothermic peak confirms favorable thermal stability, supporting transesterification use. A processing temperature of ~420 °C suffices to produce a stable nanocatalyst, consistent with previous studies on biomass thermal conversion (Abozied et al., 2024; Nallappan et al., 2021).

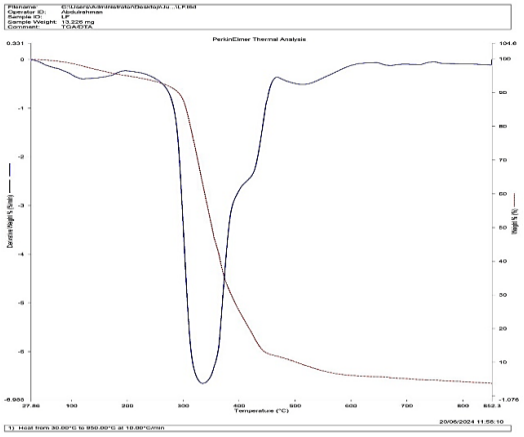

Figure 5a: Luffa fibre (TGA)

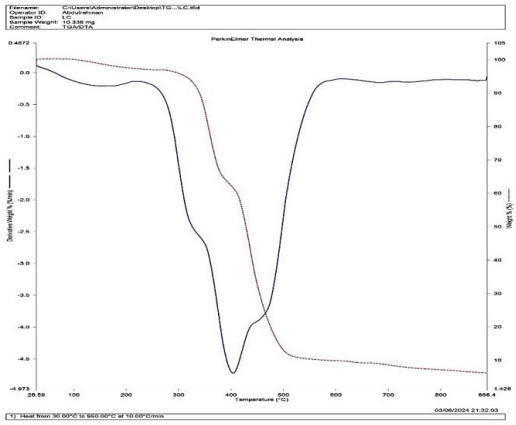

Figure 5b: Nano catalyst (TGA)

3.3 Process parameters impact

Figures 6a-c summarize the effects of catalyst concentration, reaction time, and temperature on the oxirane value of epoxidized *luffa* oil. The maximum oxirane values were observed at 1.8 mol/L catalyst (Figure 6a), 7 h reaction time (Figure 6b), and 65 °C (Figure 6c), with further increases causing declines due to oxirane ring cleavage and side reactions. The inverse relationship between iodine and oxirane values confirmed C=C conversion. Catalyst loading, time, and temperature significantly influenced oxirane formation, with time and temperature being economically critical. These trends align with prior studies on *huracrepitan*, and *Azadirachta indica* seed oils (Aguele et al., 2021; Nwosu-Obieogu et al., 2022).

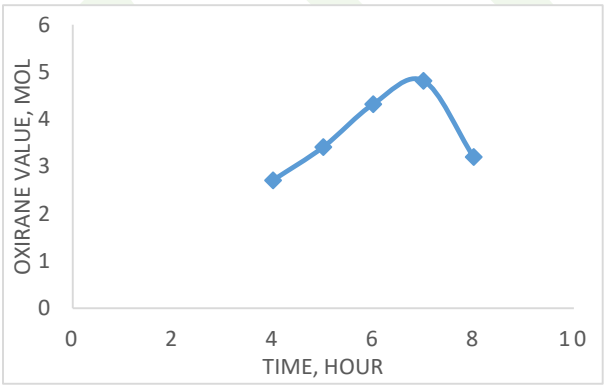

Fig. 6a: Catalyst effect on the oxirane

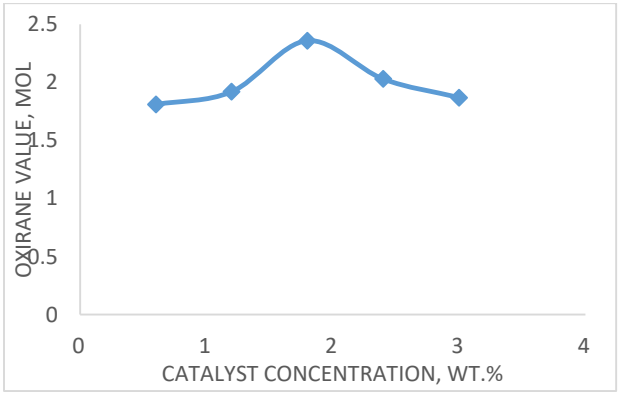

Fig. 6b: Time effect on the oxirane

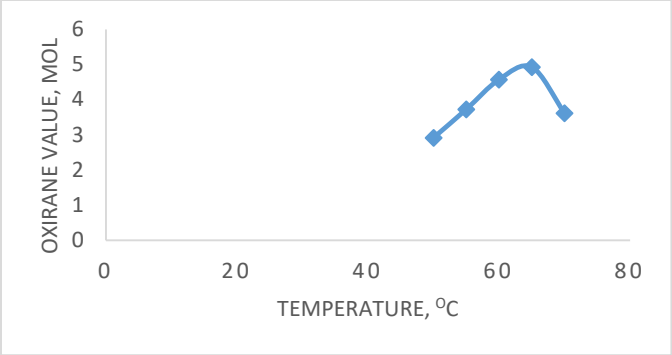

Figure 6c: Temperature's impact on the oxirane

3.4 Kinetics of epoxidation

The plot of conversion to oxirane over time at various temperature is shown in Fig. 7a. The rate of the reaction increases with a corresponding rise in temperature. At 338K, the time increased rapidly until it reached 3 hours with an oxirane value of 2.5 mol, however at a temperature of 328K and 333K, the optimal oxirane values are 2 mol and 1.75 mol respectively. At a time above 4 hours, the reaction rate is slow due to the degradation of oxirane at a higher time. The plot of $\{[H_2O_2]_0 - [EP]\}$ against time in Fig. 7b. showed a deviation from linearity with ring opening for the reactions; hence, the rate constants(0.0392, 0.1584, and 0.222) were obtained with the initial slopes at a temperature of 328, 333 and 338K respectively. The increase in rate constants as the temperature rose suggested an endothermic process, indicating that the reaction proceeds more quickly as the temperature increases due to more frequent and energetic collisions between reactant molecules; this observation favours the epoxide formation. The rate constants obtained for the reaction agreed with the report from melon seed oil (Nwosu-obieogu et al., 2024) . From Fig. 7c, the enthalpy, $\triangle H$, was determined to be 14.442KJ/mol, indicating an endothermic reaction; rising temperature could increase OOC conversion, and the entropy for the activation, $\triangle S$ = -21.75 $cal.mol^{-1}.K^{-1}$ indicating that the disorderliness in the process is less .

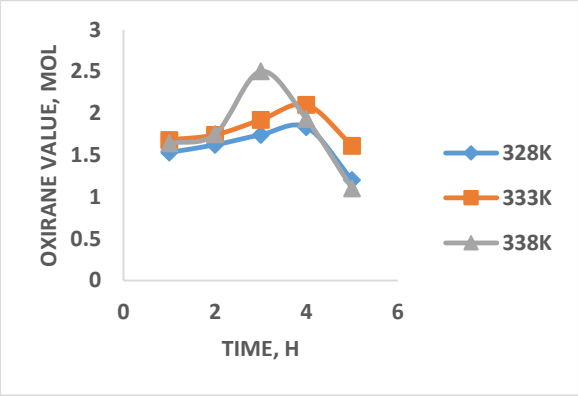

Fig. 7a. Time effect on the oxirane at various temperatures

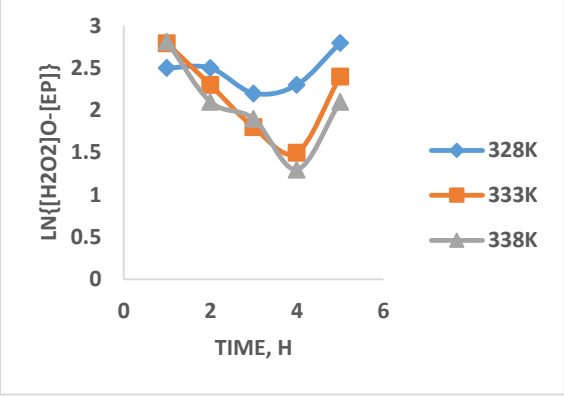

Fig. 7b. ln[H_2O-OOC] vs time

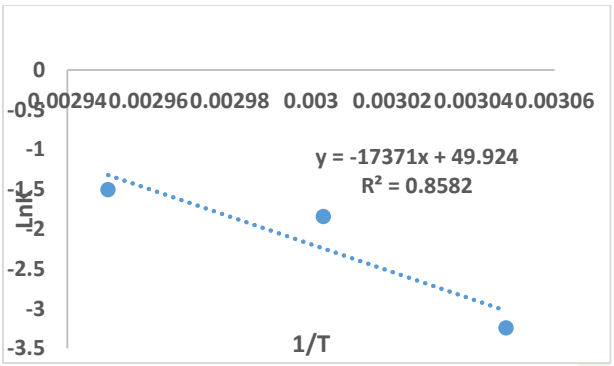

Fig. 7c. Activation energy, Ea for luffa oil epoxidation

3.5 Epoxide chacraterization

The FTIR spectrum of the epoxidized product, shown in Figure 8, exhibits a broad O–H stretching peak at 3381.9 cm^{-1}, confirming alcohol formation during the epoxidation reaction and indicating the disappearance of the original C=C bonds following sulfuric acid–assisted epoxidation. Additionally, an absorption band at 1714.6 cm^{-1} appears in the EAISO spectrum, signifying the presence of a cyclic ether group characteristic of epoxy functionality. These observations are consistent with reports by Mekonnen (2021) for *Podocarpus falcatus* oil, Oke et al. (2021) for *Hevea brasiliensis* oil.

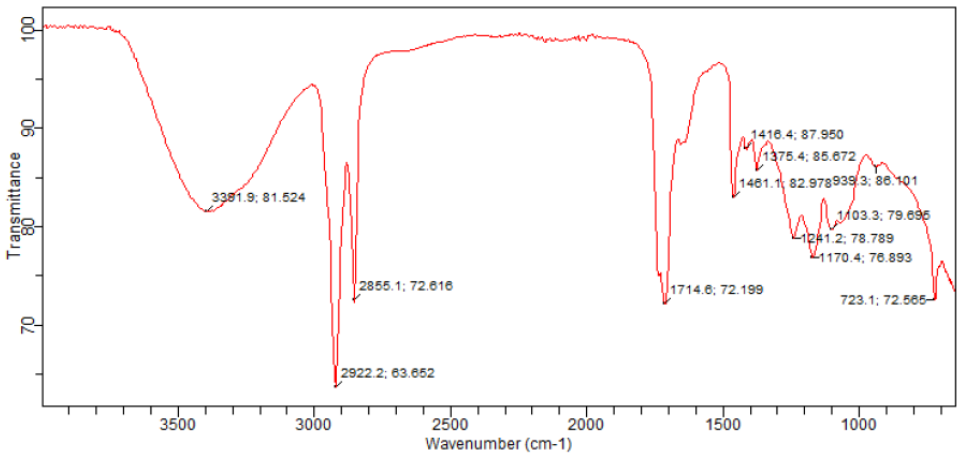

Fig. 8: FTIR for luffa epoxide

4.0 CONCLUSION

The sulfonated luffa fibre nanocatalyst exhibited enhanced surface chemistry, porosity, and nanoscale morphology, enabling efficient epoxidation of luffa seed oil. TGA and XRD confirmed thermal and structural stability under moderate conditions. Kinetics followed pseudo-first-order behavior with rate constants of 0.0392–0.222 h^{-1}, Ea = 14.44 kJ mol^{-1}, and ΔS = –21.75 cal mol^{-1} K^{-1}, indicating an ordered, endothermic pathway. Iodine value reduction and epoxy bands confirmed functionalization. Findings demonstrate luffa as a dual-use, circular feedstock for catalysts and bio-epoxides. Future studies should evaluate recyclability, turnover frequency, and scale-up in continuous-flow systems, alongside polymer.

REFERENCES

Abozied, A. M., Abouelsayed, A., Anis, B., Zayed, M. F., Eisa, W. H., & Abdelrazzak, A. B. (2024). Thymus vulgaris-assisted growth of nickel nanoparticles onto Luffa fibers: A robust and recyclable catalyst for the reduction of organic pollutants. Materials Today Sustainability, 27, 100814.

Addli, M. A., Jalil, M. J., Alrashed, M. M., Azmi, I. S., Ahmad, M. A., & Mustapha, S. N. H. (2025). Enhanced catalytic performance and recycling of sulfate-impregnated ZSM-5 in the epoxidation of castor oil. Biomass Conversion and Biorefinery, 1-28.

Aguele, F. O., Nwosu-Obieogu, K., Osoh, K. O., Onyekwulu, C. S., & Chiemenem, L. I. (2021). Optimization of the epoxidation process parameters of huracrepitan seed oil. Annals of the Faculty of Engineering Hunedoara, 19(1), 61-68.

Álvarez, M., Reilly, A., Suleyman, O., & Griffin, C. (2025). A systematic review of epoxidation methods and mechanical properties of sustainable bio-based epoxy resins. Polymers, 17(14), 1956.

Baczewska, P., Nowak, D., Jaszczewska-Adamczak, J., Bachorz, R. A., Hoffmann, M., & Mlynarski, J. (2025). Machine Learning Prediction of Enantioselectivity in Asymmetric Catalysis from Small, Curated Datasets: Case Studies in Magnesium-Catalyzed Epoxidation and Thia-Michael Addition.

Belaid, B., Khalladi, R., Cherifi, H., Yous, R., & Khachay, A. (2025). Development of high-performance activated carbons from algerian Luffa cylindrica for efficient phenol removal: A comprehensive structural, surface, and thermal characterization. Journal of Industrial and Engineering Chemistry.

Calabia, R. O. A., Gomez, J. E. D., Lasala, I. M., Ligsay, C. M. A., Maalihan, R. D., Aquino, A. P., & Sangalang, R. H. (2025). Epoxidised Philippine natural rubber for tough and versatile 3D printable resins: a mixture design and neural network approach. Journal of Rubber Research, 1-13.

Coutinho, R., Hoshima, H. Y., Vianna, M. T. G., & Marques, M. (2024). Sustainable application of modified Luffa cylindrica biomass for removal of trimethoprim in water by adsorption with process optimization. Environmental Science and Pollution Research, 31(43), 55280-55300.

De Souza, P. H. C., Rocha, S. D. F., & de Rezende, D. B. (2023). Luffa cylindrica slow pyrolysis and solar pyrolysis: impact of temperature and heating rate on biochar properties and iodine adsorption performance. Waste and Biomass Valorization, 14(5), 1753-1768.

Fernandes, C. D., de Castro, V. L. S. S., Vallim, J. H., Wani, A. K., Americo-Pinheiro, J. H. P., Serejo, T., ... & Romanholo Ferreira, L. F. (2025). Enzymatic extract from Luffa-Immobilized pleurotus sajor-caju: a promising biocatalyst for agro-Industrial pollutant reduction and toxicity mitigation. Topics in Catalysis, 68(9), 780-795.

Ferraz-Caetano, J., Teixeira, F., Cordeiro, M. N. D., & Miyao, T. (2025). Inverse ligand design: a generative data-driven model for optimizing vanadyl-based epoxidation catalysts. Journal of Catalysis, 116537.

Foroutan, R., Peighambardoust, S. J., Mohammadi, R., Peighambardoust, S. H., & Ramavandi, B. (2022). Generation of biodiesel from edible waste oil using ZIF-67-KOH modified Luffa cylindrica biomass catalyst. Fuel, 322, 124181.

Ho, Y. H., Parthiban, A., Thian, M. C., Ban, Z. H., & Siwayanan, P. (2022). Acrylated biopolymers derived via epoxidation and subsequent acrylation of vegetable oils. International Journal of Polymer Science, 2022(1), 6210128

Jin, G., Liu, B., Liu, Y., Zhang, X., Cao, D., & Zhang, X. (2025). Luffa-like Interconnective Porous Nanofiber with Anchored Co/CoCr2O4 Hybrid Nanoparticles for Zinc–Air Batteries. Batteries, 11(8), 306

Khatoon, A., Siddiqui, S., Khan, S. H., Alfaiz, F. A., & Uddin, M. K. (2025). Removal of methylene blue, crystal violet, and diclofenac sodium using cellulose derived from Luffa acutangula peels: adsorption, reusability, and cost evaluation. Biomass Conversion and Biorefinery, 1-14.

Kopal, I., Labaj, I., Vršková, J., Harničárová, M., Valíček, J., Bakošová, A., ... & Khanna, A. (2025). Predictive Modelling and Optimisation of Rubber Blend Mixing Using a General Regression Neural Network. Polymers, 17(13), 1868.

Lin, Y., Yang, C., Pei, Z., Xu, H., Zhang, Y., Ma, J., ... & Cai, J. (2025). Luffa sponge as a sustainable reinforcement for impact-resistant cementitious composites. Communications Materials, 6(1), 253.

Mekonnen, Y. (2021). Epoxidation of podocarpus falcatus oil by sulphuric acid catalyst: process optimization and physio-chemical characterization. Am. J. Chem. Eng, 9(4), 84-90.

Mukherjee, R. B., Rajput, C. V., & Chilkhaliya, N. P. (2025). A sustainable non-edible plant oil derived from Simarouba glauca (Lakshmi Taru) seed oil and its Prilezhaev epoxidation: an experimental and computational study. Biomass Conversion and Biorefinery, 15(12), 19043-19068.

Nallappan, D., Fauzi, A. N., Krishna, B. S., Kumar, B. P., Reddy, A. V. K., Syed, T., ... & Rao, P. V. (2021). Green biosynthesis, antioxidant, antibacterial, and anticancer activities of silver nanoparticles of Luffa acutangula leaf extract. BioMed Research International, 2021(1), 5125681.

Nwosu-Obieogu, K., Agu, C. M., Dzarma, G. W., Awele, A. M., & Nkemakolam, A. (2022). Microwave-assisted carbon-based sulphonated melon seed peel catalyst development for the optimization of neem seed oil epoxidation using response surface methodology. Cleaner Materials, 4, 100069.

Nwosu-Obieogu, K., Allen, M. A., Nwogu, C., Nwankwojike, B., Bright, S., & Goodnews, C. (2025). L uffa oil transesterification prediction via adaptive neuro-fuzzy inference system using an acid-activated waste marble catalyst. Proceedings of the Indian National Science Academy, 91(1), 299-311.

Nwosu-Obieogu, K., Goodnews, C., Dzarma, G. W., Ugwuodo, C., & Gabriel, O. (2024). Azadirachta indica seed oil epoxidation process using carbonized melon seed peel catalyst; genetic algorithm coupled artificial neural network approach. South African Journal of Chemical Engineering, 49, 258-272.

Nwosu-Obieogu, K., Grace, E., Adekunle, K. F., Chiemenem, L. I., Aguele, F. O., & Dzarma, G. W. (2022). In-situ selective epoxidation of Colocynthis Vulgaris shrad seed oil for the synthesis of a methacrylated biobased resin; An artificial neural network (ANN) modelling approach. Cleaner and Circular Bioeconomy, 3, 100028.

Nwosu-Obieogu, K., Grace, E., Dzarma, G. W., Aguele, F. O., Chiemenem, L. I., Gabriel, O., and Ekeoma, N. (2024). Melon seed oil epoxidation: kinetics and neuro-fuzzy evaluation. South African Journal of Chemical Engineering, 47(1), 169-177.

Nwosu-Obieogu, K., Oke, E., Adeyi, O., Dzarma, G. W., Felix, A., Linus, C., ... & Goodnews, C. (2024). Azadirachta indica Seed Oil Epoxidation Using Sulfuric Acid as a Catalyst; Response Surface Methodology and Particle Swarm-Based Evaluation and Optimization. Transactions of the Indian National Academy of Engineering, 9(4), 951-964.

Oke, E. O., Nwosu-Obieogu, K., Okolo, B. I., Adeyi, O., Omotoso, A. O., & Ude, C. U. (2021). Hevea brasiliensis oil epoxidation: hybrid genetic algorithm–neural fuzzy–Box–Behnken (GA–ANFIS–BB) modelling with sensitivity and uncertainty analyses. Multiscale and Multidisciplinary Modeling, Experiments and Design, 4(2), 131-144.

Oyelaran, O. A., Sanusi, O., Borisade, S., Abioye, J., & Olumoroti, I. (2022). Physiochemical and Electrical Properties of Refined Luffa (Luffa Cylindrica) Seed Oil as Bio-Transformer Oil. El-Cezeri, 9(1), 133-143.

Paula, E. A., Melo, R. R. D., Silva Jr, M. Q., Paula, Y. L., Pimenta, A. S., Souza, J. A. G., and Rodolfo Jr, F. (2022). Characterization of polyester composites reinforced with natural fibers from Luffa cylindrica. Journal of Composite Materials, 56(28), 4313-4327.

Prasannakumar, P., Santhakumari, R., Thampi, A. D., Sneha, E., Adithyan, K. S., & Sabarinath, S. (2024). Epoxidation of Calophyllum inophyllum oil fatty acid methyl esters as a potential base-stock for green cutting fluid. Environment, Development and Sustainability, 1-25.

Rahman, S. J. A., Jalil, M. J., Riduan, M. A., Ibrahim, I. M., & Azmi, I. S. (2025). Catalytic epoxidation of palm oil-derived oleic acid using TiO2: A sustainable approach. Environmental Progress & Sustainable Energy, e70067.

Santos, M. A., De Conto, J. F., Borges, G. R., & Egues, S. M. (2024). Luffa cylindrica as a biosorbent in wastewater treatment applications: a comprehensive review. Cellulose, 31(17), 10115-10142.

Varghese, T. P., Reghunadhan Nair, C. P., and Gopalakrishnan, J. (2025). Green Epoxidized Niepa Seed Oil for Toughening Epoxy Resin: An Insight Into Viscoelastic, Mechanical, Thermal and Adhesive Properties. Polymer Engineering & Science.

Zhang, J., Wu, S., Xu, R., Wang, C., Li, C., Hao, J., ... & Chen, Y. (2021). A study on natural luffa seed oil as a potential source of polymers and bioactive compounds. Industrial Crops and Products, 171, 113895.

Zhou, J., Wu, S., Zhang, C., Shan, H., Ling, G., Xu, R., ... & Chen, Y. (2024). High-performance bio-based foam from agricultural waste luffa seed oil polyols. Materials Today Communications, 41, 110438.

To cite this article:
Prince Chinaemeze Iroabueke and Kenechi Nwosu-Obieogu, 2026. Kinetic Evaluation of the Epoxidation of Luffa *Cylindrica* M. Seed Oil Utilizing *Luffa* Fibre Catalyst. 1(2): 20-32. https://journals.unizik.edu.ng/ujabe/